NONLINEAR SELF-EXCITED THERMOACOUSTIC OSCILLATIONS OF A DUCTED PREMIXED FLAME: BIFURCATIONS AND ROUTES TO CHAOS

Karthik Kashinath*[1], Iain C. Waugh[1], Matthew P. Juniper[1]

[1] Cambridge University Engineering Department, Trumpington Street, Cambridge - CB2 1PZ, United Kingdom
* Corresponding author: kk377@cam.ac.uk

We study the bifurcations of a ducted two-dimensional premixed flame using numerical simulations of the coupled dynamical system. When the flame position in the duct is changed the system undergoes transition to period-*1*, quasi-periodic, period-*2*, frequency-locked and chaotic oscillations via different bifurcations. For certain parameter ranges multiple stable solutions exist and the ultimate state reached depends on the initial conditions. Hence there is hysteresis and mode switching is possible. Often the system traverses through intermediate states before reaching its final stable state. Two routes to chaos are established for this system: the period-doubling route and the Ruelle-Takens-Newhouse route. Flame images show that the flame wrinkles have multiple time and length scales, which reflect the nonlinear behaviour seen in the time series. This study complements recent experiments by providing a reduced order model with approximately 5000 degrees of freedom that captures much of the complex nonlinear dynamics observed in the laboratory.

Most studies of nonlinear thermoacoustics assume that the oscillations are periodic with a dominant frequency and a fixed amplitude, in other words, they assume that the system always reaches a period-*1* limit cycle. Recent experiments, however, reveal that even simple thermoacoustic systems exhibit nonlinear behaviour that can be far more complicated than period-*1* limit cycle oscillations [1–3]. By varying a control parameter in their thermoacoustic system, Kabiraj *et al.* show that the system undergoes several bifurcations resulting in a variety of nonlinear oscillations including quasi-periodic, frequency-locked and chaotic oscillations [1]. Experiments in large industrial scale thermoacoustic systems by Gotoda *et al.* reveal that as the equivalence ratio increases, the thermoacoustic behaviour undergoes a significant transition from stochastic fluctuations to periodic oscillations through low-dimensional chaotic oscillations [4].

A few models do not assume *a priori* that the system reaches period-*1* oscillations [5–8]. But these models generally assume that the unsteady heat release rate is a simple, often polynomial, function of the pressure or velocity fluctuations, so that the study may be analytically tractable. This assumption, however, is unrealistic because the heat release rate of flames depends not only on the instantaneous acoustic pressure or velocity, but also on historical values, because a flame has memory [9]. The current flame shape and heat release rate depends on the integrated effect of past perturbations. Hence, simple analytical descriptions of heat release rate that do not account for memory effects cannot capture the complexities of unsteady flame dynamics.

In this study, therefore, we use a more realistic flame model with simple duct acoustics and do not assume *a priori* that the system reaches a period-*1* oscillation. We investigate the nonlinear dynamics of a ducted two-dimensional premixed flame using numerical simulations of the coupled nonlinear dynamical system. This resembles the thermoacoustic system that has recently been investigated in detail experimentally by Kabiraj *et al.* but differs in the fact that we use a 2-D flame and not an axisymmetric

one [3]. We use techniques and well-established results from dynamical systems theory and nonlinear time series analysis to understand the nonlinear behaviour of this system.

This study relies on analyses of the time series from several simulations of the coupled system for different parameter values and initial conditions. This is a time-consuming process. Continuation techniques are more efficient at tracking limit cycles and their bifurcations. Waugh has developed a matrix-free continuation method for a similar thermoacoustic system with an axisymmetric flame [10] and shown in a separate paper in this conference how this technique can provide insights into the behaviour of the coupled nonlinear system [11].

1 The Thermoacoustic Model

We focus on the nonlinear dynamics of the flame, keeping the acoustic system simple. In this study we consider a duct open at both ends with a two-dimensional laminar premixed flame located at a distance $\tilde{x}_f$ from one end. The acoustics can be treated linearly even for large acoustic velocity fluctuations because the perturbation Mach number remains small [12]. A compact flame assumption is used here because we assume that the flame length is small compared to the wavelengths of the duct's acoustic modes. The governing equations in dimensional and non-dimensional form have been described in detail in previous studies that have used the same acoustic model [**?**, 13]. In this formulation we have not accounted for the effect of temperature change across the flame on the acoustic modeshapes and frequencies. This is a reasonable assumption, however, because the flame occupies a small fraction of the cross-section of the duct (0.2), although this means quantitative comparisons with experiments are not possible.

The flame is described by the kinematic G-equation model using a level set approach. The principal assumptions of the model are that (1) the flame is a thin surface separating unburnt reactants from burnt products; (2) the influence of gas expansion across the flame front is negligible. These simplifications allow the flame to be modelled with a much smaller system than would be required for fully-resolved CFD. Assumption (1) allows for the flame to be tracked using the G-equation, which we have described in detail in our previous studies [14, 15]. Assumption (2) allows for the velocity field to be independently specified, neglecting the effect that the heat release has on the flow-field. In a coupled self-excited system as in the present study, however, the velocity field around the flame is perturbed by the acoustic field at the burner.

Studies of acoustically forced premixed flames have shown that acoustic waves induce velocity perturbations at the base of the flame [16, 17]. These velocity perturbations then travel along the flame, distorting its surface and therefore causing flame area fluctuations that result in unsteady heat release rate oscillations. Therefore the perturbation velocity is modelled as a travelling wave that originates at the burner lip [18]. Experiments on laminar premixed flames [19] and direct numerical simulations in our previous work [15] have shown that the phase speed of these velocity perturbations is not equal to the mean flow. It is a function of the forcing frequency but is independent of the forcing amplitude. Furthermore, we found that for a slot-stabilized 2-D premixed flame it is usually less than the mean flow in the range of frequencies relevant to thermoacoustic oscillations.

The acoustic perturbations in this study are non-harmonic and therefore we cannot use a frequency-dependent phase speed because the frequencies are not known *a priori*. So we assume a constant phase speed, but one that is different from the mean flow. Accordingly, the non-dimensional streamwise perturbation velocity field may be found by solving the 1-D advection equation,

$$\frac{\partial u}{\partial t} + \frac{1}{K}\frac{\partial u}{\partial x} = 0 \tag{1}$$

where, $K = \tilde{u}_0/\tilde{u}_c$ is the ratio of the mean flow velocity to the phase speed of velocity perturbations. In our previous work we have shown that K has a strong effect on the nonlinear behaviour and that subcritical bifurcations exist only for $K > 1$ [14, 15]. We assume $K = 1.1$ in this study. The boundary condition is that the velocity perturbation in the flame domain at the burner lip equals the acoustic velocity at the flame position, $u(x_{burner}, t) = u_{acoustic}(x_f, t)$. Therefore the axial velocity at a point in the flame domain is the delayed acoustic velocity at the flame position, with a delay equal to the time

taken for the travelling wave to propagate from the burner to that point. As in our previous work [15,20], we solve the continuity equation within the flame domain to find the transverse velocity perturbation field.

We have chosen to anchor the base of the flame to the burner lip. Recent experiments on a self-excited ducted premixed flame show that flame lift-off occurs at large velocity fluctuation amplitudes and can lead to complicated nonlinear behaviour such as intermittency, ultimately leading to flame blow-out [3]. This cannot be captured in our model. Flash back, however, is allowed to occur using the boundary condition proposed by Dowling [21] and implemented in the level set solver by Waugh [10]. We have neglected in the influence of curvature on the flame speed in this study, but this has been included in a continuation analysis of a similar thermoacoustic system by Waugh [10]. Neglecting curvature effects on the flame speed results in very sharp cusps on the flame surface, which is unrealistic. This, however, allows faster computations because curvature is a second order quantity that requires a much smaller timestep for numerical stability.

For premixed flames with constant flame speed, the heat release rate is proportional to the flame surface area, which is calculated as in previous studies [14, 15, 22]. The simple velocity model we use here results in an unsteady heat release rate whose mean is less than the steady heat release rate of the unperturbed flame, which is unphysical. The thermoacoustic oscillations are not affected by the mean heat release rate, however, so this simple model is retained.

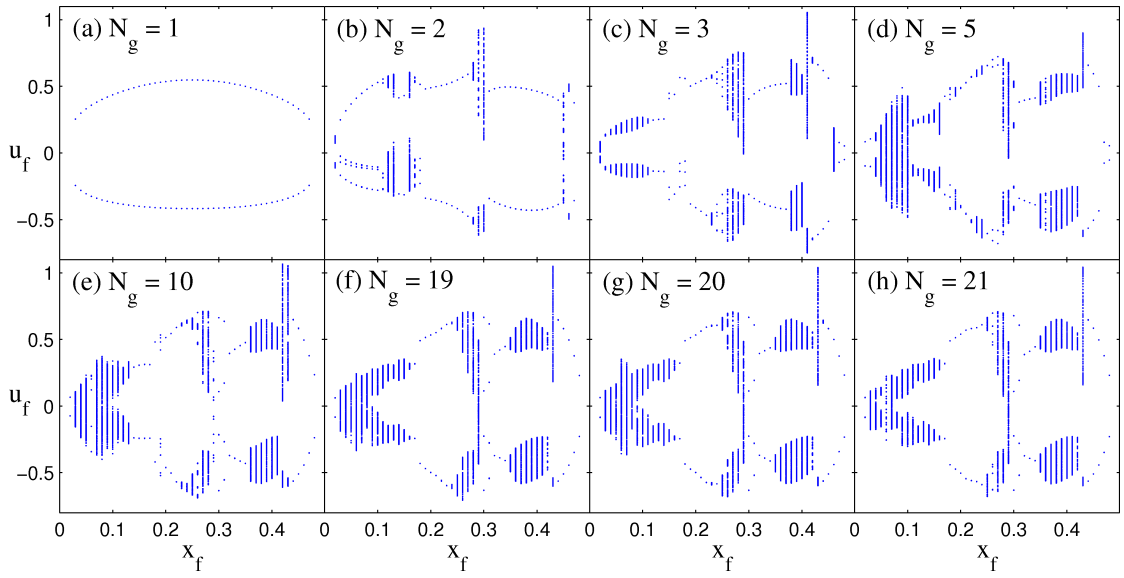

Figure 1: Bifurcation diagrams with flame position, x_f, as control parameter with different numbers of Galerkin modes, N_g, in the discretization: (a) $N_g = 1$, (b) $N_g = 2$, (c) $N_g = 3$, (d) $N_g = 5$, (e) $N_g = 10$, (f) $N_g = 19$, (g) $N_g = 20$ and (h) $N_g = 21$. At a given value of x_f the points on the diagrams are the peaks and troughs of the velocity time series data once the system has reached a stable state. (a) shows that for $N_g = 1$ the system always reaches a period-*1* limit cycle. As the number of modes is increased modal interactions result in more complicated solutions such as period-*2*, frequency-locked and quasi-periodic solutions. Further, the maximum amplitudes of oscillations are significantly higher than the single-mode case (a). Comparing (f), (g) and (h) shows that the solutions are independent of the discretization when N_g is sufficiently large.

The evolution equations of the coupled nonlinear system: the *G*-equation, the acoustic equations and perturbation velocity equations are solved simultaneously numerically using a WENO 5th order scheme in space [23] with a 3rd order TVD Runge-Kutta scheme [24] for time integration. The non-dimensionalized spatial and temporal resolution in all the simulations are 5×10^{-3} and 10^{-3} respectively, with a uniform mesh spacing in both spatial directions. For the *G*-equation computations, the local level set method is used to achieve a significant reduction in computational cost [25] and is solved

using LSGEN2D, a general level set method solver, developed by Hemchandra [26] with extensions and modifications by Waugh [10].

2 Results

2.1 Bifurcation diagrams

The qualitative nature of a nonlinear dynamical system is best described by the bifurcation diagram, which shows the changes in the nature of solutions to the governing equations as a control parameter changes. The number of Galerkin modes used in the discretization of the acoustic equations affects the interactions between different acoustic modes and therefore the solutions of the governing equations. When there is more than one Galerkin mode, there can be energy transfer between the modes via the heat release rate term in the energy equation, resulting in a more complex behaviour and a non-harmonic acoustic waveform.

Figure 1 shows bifurcation diagrams with flame position, x_f, as control parameter using different numbers of Galerkin modes, N_g. At a given value of x_f the points on the diagrams are the peaks and troughs of the velocity time series data once the system has reached a stable state. We choose the velocity at the flame position as this is most relevant for the flame dynamics.

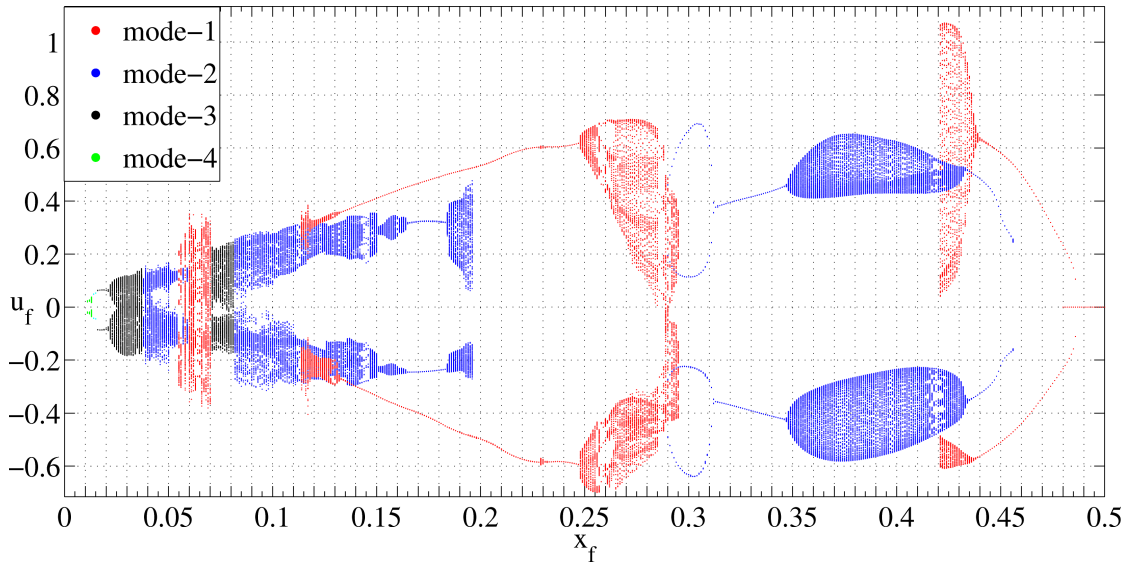

Figure 2: Bifurcation diagram with flame position, x_f, as control parameter. The u_f values are the peaks and troughs of the time-series once the system has settled to its final stable state. One set of points was obtained by increasing x_f starting from the stable state at the previous x_f. The other set of points was obtained by decreasing x_f. The different colours represent the most dominant acoustic mode in the power spectra; mode-1 is shown in red, mode-2 in blue, mode-3 in black and mode-4 in green. Other parameter values are $\phi_{mean} = 0.85$, $L_f/R = 7$, $L_f/ML_0 = 2.2$, $K = 1.1$. The sequence of bifurcations are explained in the text. This chart shows that the system can have stable period-*1*, period-*2*, period-4, frequency-locked, quasi-periodic and chaotic states depending on the x_f and initial conditions. There are several bi-stable regions, hence the system has hysteresis and mode-switching is possible.

Figure 1(a) shows that for just one mode in the acoustics the system always reaches a period-*1* limit cycle. The maximum oscillation amplitude occurs at $x_f = 0.25$ and is about one half of the mean flow. In our previous work we have shown that period-*1* limit cycles obtained in the frequency domain using a flame describing function (FDF) approach are the same as those obtained in the time domain using a single Galerkin mode in the discretization [14]. This is because the FDF approach is quasi-linear and

ignores the contribution of harmonics in the heat release rate to the acoustic velocity and pressure, as is the case when only one mode is used for the discretization. Furthermore, by definition, the FDF approach cannot include modal interactions.

As the number of modes is increased we see that modal interactions result in more complicated solutions such as period-*2*, frequency-locked and quasi-periodic solutions. Further, the amplitudes of oscillations are significantly higher than the single-mode case. This shows that even though the amplitudes of oscillations in the higher modes are very small because they are heavily damped, they have a strong effect on the oscillation amplitude and the nature of solutions of the whole system.

Comparing subfigures (f), (g) and (h), *i.e.* N_g = 19, 20 and 21, we see that the solutions are nearly independent of the discretization when N_g is sufficiently large. We have used 20 modes for the rest of the simulations in this study.

Finally, it is interesting to see that just a few modes (3 to 5) are necessary to capture most of the complicated features seen in the fully converged solution using 20 modes (Fig. 1(g)). This is promising for time domain computations. In the frequency domain, however, it is not trivial to extend the FDF approach to include the effect of modal interactions because this requires forcing the flame at multiple frequencies simultaneously to capture the response of the flame to non-harmonic inputs.

Figure 2 shows the bifurcation diagram with flame position, x_f, as control parameter. One set of points was obtained by increasing x_f starting from the stable state at the previous x_f. The other set of points was obtained by decreasing x_f. The different colours represent the most dominant acoustic mode in the power spectra.

The sequence of bifurcations from right to left (decreasing x_f) are: subcritical Hopf from a stable fixed point to an unstable period-*1* oscillation at $x_f = 0.48$, fold bifurcation from an unstable to a stable period-*1* oscillation (mode-1) at $x_f = 0.487$, supercritical Neimark-Sacker to quasi-periodic oscillations at $x_f = 0.435$. This branch of solutions (mode-1) loses stability at $x_f = 0.42$ and the system tends to quasi-periodic oscillations with a dominant frequency near that of mode-2. This branch of solutions (mode-2) has a fold bifurcation at $x_f = 0.456$, beyond which the system falls back to the mode-1 branch via an unstable period-*1* attractor. Therefore $0.42 < x_f < 0.456$ is a bistable region which shows that the system has hysteresis and that mode switching is possible in this range of x_f.

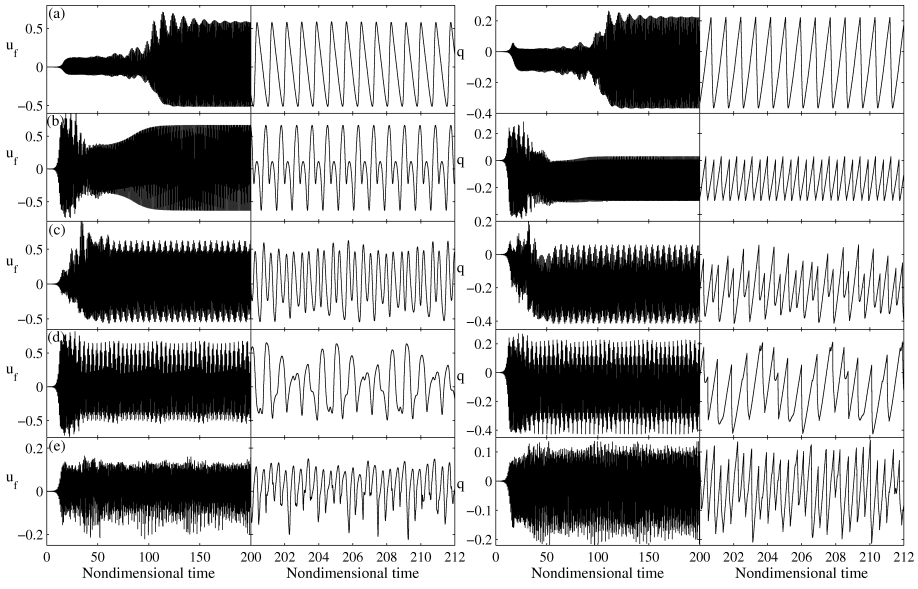

Figure 3: Time series of velocity and heat release rate for the different types of oscillation corresponding to different flame positions of figure 2: (a) period-*1* oscillation at $x_f = 0.45$, (b) period-*2* oscillation at $x_f = 0.3$, (c) quasi-periodic oscillation at $x_f = 0.4$, (d) frequency-locked oscillation at $x_f = 0.286$ and (e) chaotic oscillation at $x_f = 0.046$

In the narrow band of $0.418 < x_f < 0.42$ on the mode-2 branch the system has frequency-locked

solutions. For $0.347 < x_f < 0.418$ the solutions are quasi-periodic and this branch goes to a period-*1* oscillation via a supercritical Neimark-Sacker bifurcation at $x_f = 0.347$. The system undergoes a period-doubling bifurcation at $x_f = 0.311$ to period-*2* oscillations, which lose stability at $x_f = 0.289$ and the system switches back to mode-1 dominant quasi-periodic oscillations via an unstable quasi-periodic attractor. $0.289 < x_f < 0.296$ is a bistable region where quasi-periodic and period-*2* oscillations co-exist. Similar features are noticed for $0 < x_f < 0.289$.

Importantly, between $x_f = 0.03$ and $x_f = 0.1$ there exist bands of chaos with different strange attractors. For sizeable intervals of x_f at least two stable attractors co-exist and the final state reached by the system depends on the initial conditions. Hence the system shows hysteresis and mode-switching is possible in these multi-stable regions.

2.2 Nonlinear time series analyses

Figure 3 shows time series of the acoustic velocity at the flame position normalised by the mean flow velocity, U_0, and the heat release rate normalised by the mean heat release, $\dot{Q}_0$, for the different types of oscillation corresponding to different flame positions of figure 2: (a) $x_f = 0.45$, (b) $x_f = 0.3$, (c) $x_f = 0.4$, (d) $x_f = 0.286$ and (e) $x_f = 0.046$. The initial condition is the steady unperturbed flame. In all cases the system is linearly unstable and perturbations grow exponentially before nonlinear effects come into play and the system settles on an attractor.

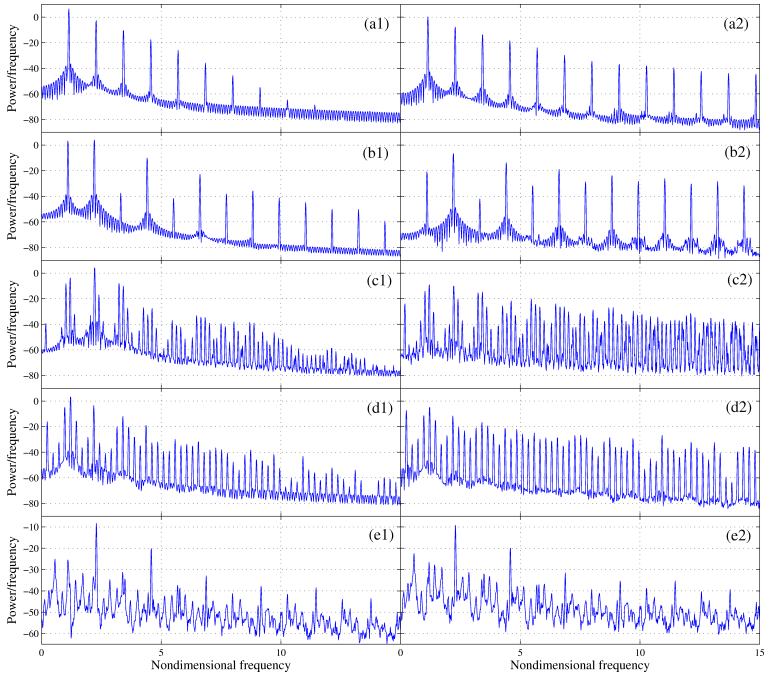

Figure 4: Power spectra of velocity (labelled 1) and heat release rate (labelled 2) for the different types of oscillation in figure 3: (a) period-*1* oscillation at $x_f = 0.45$, (b) period-*2* oscillation at $x_f = 0.3$, (c) quasi-periodic oscillation at $x_f = 0.4$, (d) frequency-locked oscillation at $x_f = 0.286$ and (e) chaotic oscillation at $x_f = 0.046$

In figure 3(a) the system is first attracted towards an unstable period-*1* oscillatory state before being repelled, and finally settling on a period-*1* attractor. The velocity and heat release rate oscillations are not sinusoidal, but they are periodic. In figure 3(b) the system is first attracted towards an unstable quasi-periodic oscillatory state before being repelled, and finally settling on a period-*2* attractor, where the oscillations alternate between a large and a small cycle. Such behaviour cannot be captured in models that assume a single dominant frequency in the acoustic velocity, such as the describing function approach. In figure 3(c) the system settles on to a quasi-periodic attractor, where the oscillations

never repeat themselves. In figure 3(d) the system is first attracted towards an unstable quasi-periodic oscillatory state before being repelled, and finally settling on a frequency-locked attractor, where the oscillations repeat themselves every few cycles, in this case, every five cycles. In figure 3(e) the system settles on to a chaotic attractor, where the oscillations never repeat themselves, *i.e.* they are aperiodic.

Figure 4 shows power spectra of the velocity (a1 to e1) and heat release rate (a2 to e2) time series shown in figure 3. The spectra are calculated using a long duration time series (300 nondimensional time units) after the system has reached its stable state. Figure 4(a) shows that spectra of period-*1* oscillations have a dominant frequency and its higher harmonics because the signal is not sinusoidal. The higher hamonics in the velocity spectrum (a1) are weaker compared to those in the heat release rate spectrum (a2) because high frequencies are strongly damped in the acoustic model. Figure 4(b) shows that spectra of period-*2* oscillations have a dominant peak and a second peak at exactly half the frequency, and their higher harmonics. Figure 4(c) shows that spectra of quasi-periodic oscillations are characterised by two frequencies that are incommensurate with each other. Side bands around the higher harmonics of the most dominant frequency are present due to nonlinear interactions between the two incommensurate frequencies. These secondary peaks are seen at frequencies that are linear combinations of the two incommensurate frequencies. Figure 4(d) shows that spectra of frequency-locked oscillations are characterised by two frequencies that are commensurate with each other. As in Figure 4(c), the side bands are due to nonlinear interactions. Figure 4(e) shows that spectra of chaotic oscillations are noisy and generally broadband with peaks at certain frequencies that are close to the natural acoustic frequencies of the duct.

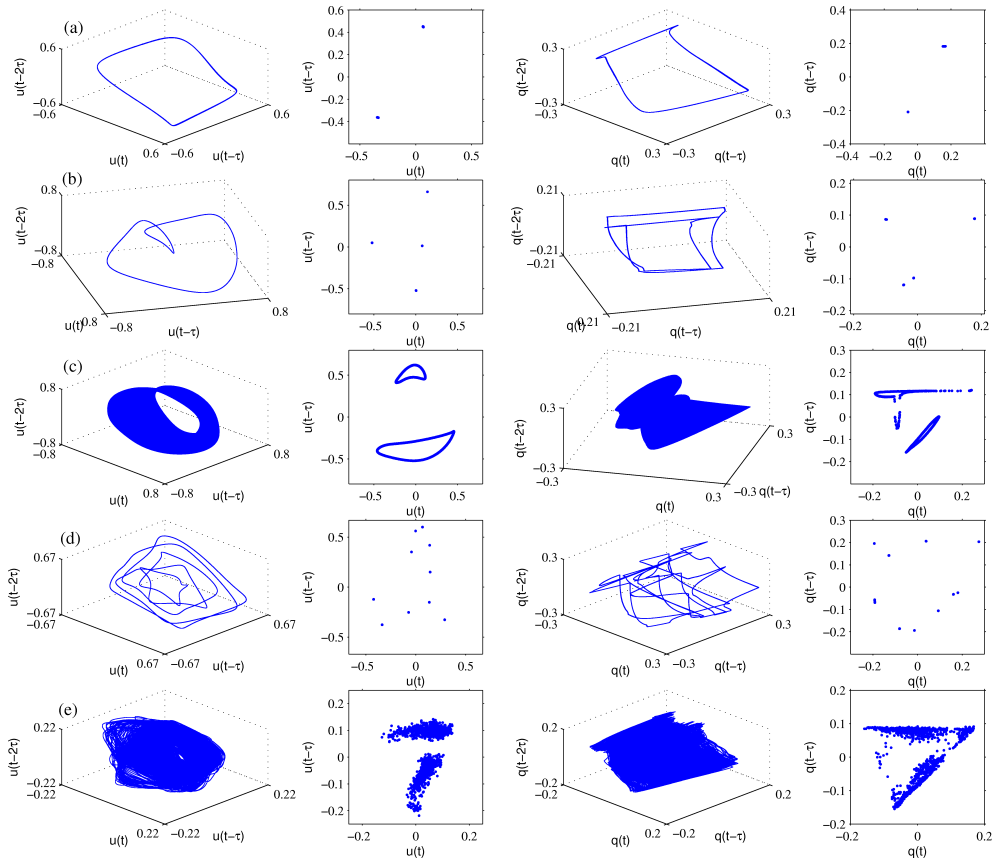

Figure 5: Phase portraits and Poincaré sections of velocity and heat release rate for the different types of oscillation corresponding to the timeseries of figure 3: (a) period-*1* limit cycle oscillation at $x_f = 0.45$, (b) period-*2* oscillation at $x_f = 0.3$, (c) quasi-periodic oscillation at $x_f = 0.4$, (d) frequency-locked oscillation at $x_f = 0.286$ and (e) chaotic oscillation at $x_f = 0.046$.

A phase space diagram can be reconstructed from the time series using the methods described in the literature on nonlinear time series analysis [27]. The Poincaré section is a transverse section of the phase portrait and has the same stability properties as the flow and shows unique characteristics for every type of attractor [28]. Figure 5 shows the phase portraits and Poincaré sections of the velocity (on the left) and heat release rate (on the right) for the different types of oscillation seen in figures 3 and 4, after the system has reached its stable state.

Figure 5 shows that periodic oscillations (or limit cycles), *i.e.* (a), (b) and (d), are closed loops in phase space. A period-*1* oscillation, (a), is a single loop, a period-*2* oscillation, (b), is a double loop and a frequency-locked oscillation, (d), is a k-loop where k is the least common multiple of the two commensurate frequencies that characterise the oscillation. Their corresponding Poincaré sections have two points, four points or $2k$ points. Figure 5(c) shows that quasi-periodic oscillations are tori in phase space, in this case 2-tori because the oscillations have two incommensurate frequencies. On a quasi-periodic attractor the system never repeats itself and hence spans the entire surface of the torus, as is implied by the closed loops of the corresponding Poincaré section. Figure 5(e) shows that chaotic oscillations appear to fill an entire volume in phase space and an area in the Poincaré section.

It is clear that the phase portraits and Poincaré sections represent the different types of oscillation in a clear and distinct way and hence are useful tools in time series analyses of dynamical systems.

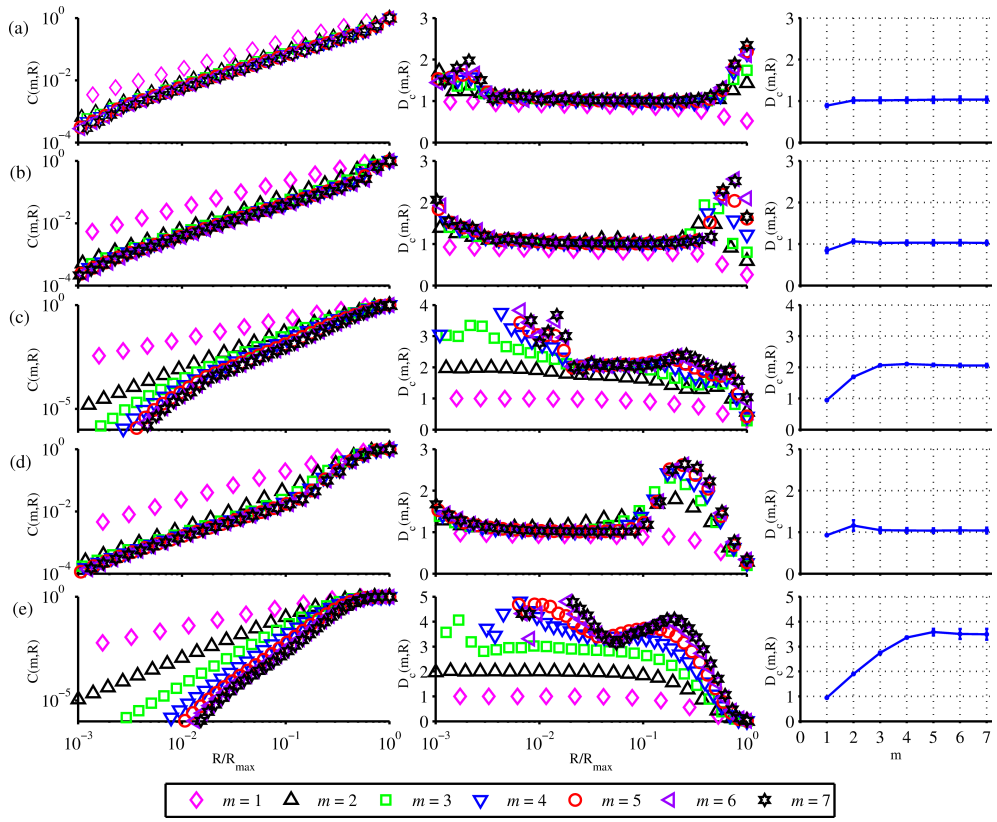

Figure 6: This figure shows the correlation sum, $C(m,R)$ (left column), and its local slope, $\partial \log C(m,R)/\partial \log R$ (middle column), as functions of the Euclidean distance, R/R_{max}, for an embedding dimension up to $m = 7$. Shown in the right column is the correlation dimension defined as the average slope $(\overline{\partial \log C(m,R)/\partial \log R})$, over the range of radii where the slope remains fairly constant, as a function of the embedding dimension, m. (a) through (e) correspond to period-*1*, period-*2*, quasi-periodic, frequency-locked and chaotic oscillations respectively. (a) to (d) are at the same operating conditions as (a) to (d) of Fig. 3, while (e) has the same conditions as Fig. 3(e), except that L_f/ML_0=1.88 and $x_f = 0.4$ for this case.

The correlation dimension measures the number of active degrees of freedom in a dynamical system and is used to determine the nature of an attractor [27]. We use the algorithm of Grassberger & Procaccia [29] implemented in the online package TISEAN by Hegger *et al.* [30], with up to 7 embedding dimensions. Figure 6 shows the correlation sum and its local slope as functions of the Euclidean distance for an embedding dimension up to 7. On the right is the correlation dimension defined as the average slope over the range of radii where the slope remains fairly constant, as a function of the embedding dimension. For periodic oscillations (a, b and d), the correlation dimension and hence the number of degrees of freedom is 1. For quasi-periodic oscillations (c) it is 2 and for chaotic oscillations (e) it is not an integer, in this case 3.5 ± 0.2.

2.3 The role of unstable attractors

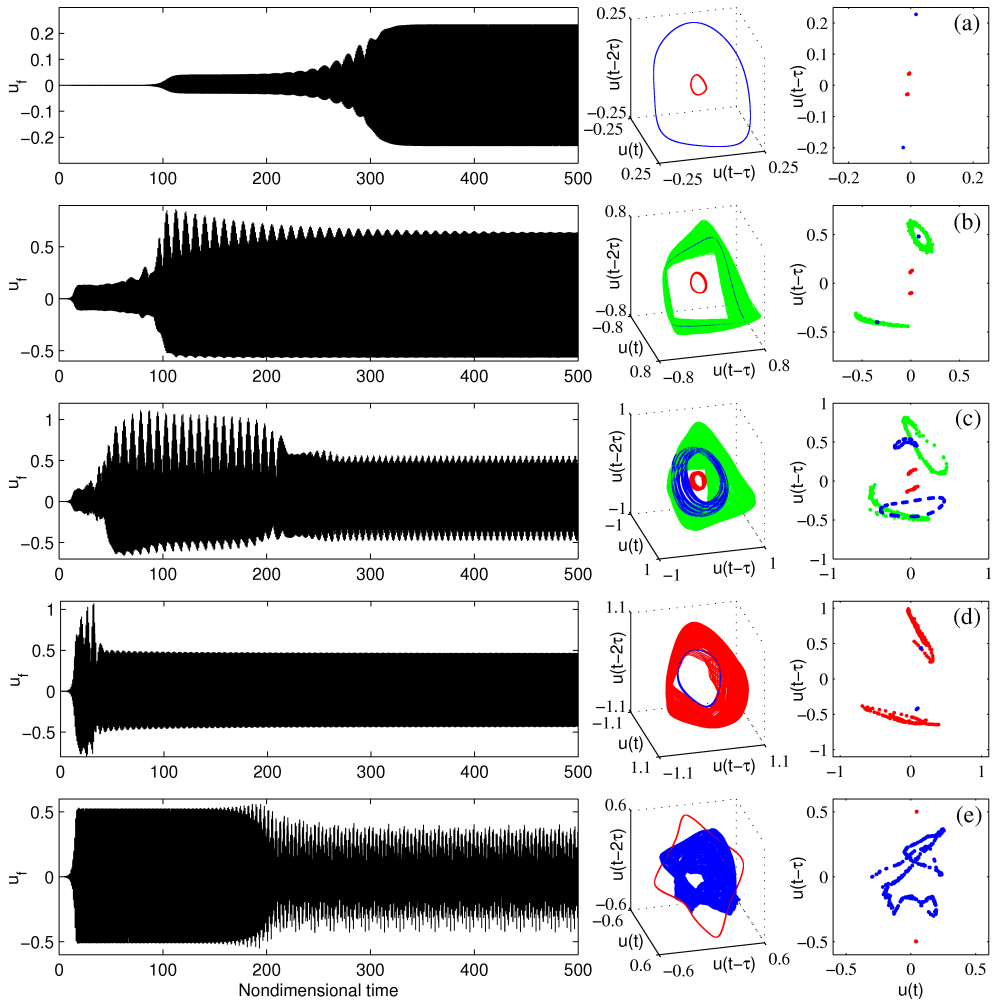

Figure 7: The time series, phase portraits and Poincaré sections of trajectories starting from the steady base state to the final stable state with one or more intermediate states: (a) $x_f = 0.480$, (b) $x_f = 0.440$, (c) $x_f = 0.420$, (d) $x_f = 0.347$ and (e) $x_f = 0.2651$. For (a) to (d) $L_f/ML_0 = 2.2$ and for (e) $L_f/ML_0 = 2.0$. The following windows of the time series are used to extract the intermediate states: (a) $120 < t < 200$ and $350 < t < 500$, (b) $40 < t < 60$, $110 < t < 150$ and $400 < t < 500$, (c) $25 < t < 35$, $100 < t < 180$ and $300 < t < 500$, (d) $10 < t < 20$ and $100 < t < 500$, (e) $40 < t < 140$ and $250 < t < 500$. The final stable state is shown in blue.

Figure 7 shows the time series, phase portraits and Poincaré sections of trajectories starting from the

steady base state to the final stable state via intermediate states. These intermediate states are close to the unstable attractors of the system. Trajectories in the neighbourhood of unstable attractors are attracted towards them in some directions but repelled in others. Unstable attractors partition the phase space into basins of attraction of different attractors. Identifying the unstable attractors of a dynamical system is crucial because bifurcations occur at the intersections of stable and unstable manifolds, which are the basins of attraction of stable and unstable attractors [31].

The phase portraits of sections of the time series are used to identify these unstable states. In figure 7(a) the system is first attracted towards an unstable period-*1* limit cycle (red) and then repelled by it to a stable period-*1* limit cycle of larger amplitude (blue). In (b) the system is attracted towards the same unstable period-*1* limit cycle as in (a) and then repelled away. Before it settles on a stable period-*1* limit cycle (blue), there is a slow decay of one of the components of the perturbation. In (c) the initial behaviour similar to that in (b) but here the system lingers around an unstable quasi-periodic period state (green) for a long time before it is repelled to its final quasi-periodic state. This shows that the first quasi-periodic state (green) is unstable. In (d) the system is strongly attracted from its steady base state towards a quasi-periodic state (red) and equally strongly repelled away from it to finally settle on to a stable period-*1* limit cycle. In (e) the path to the stable quasi-periodic state (blue) is via an unstable period-*1* limit cycle (red) of a large amplitude.

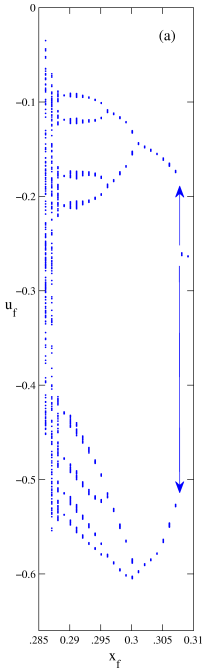

Figure 8: Period doubling route to chaos: bifurcation diagram

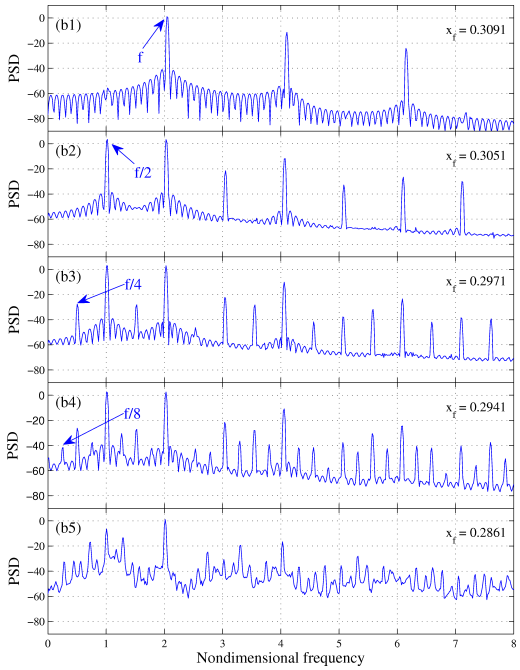

Figure 9: Period doubling route to chaos: PSD of u_f showing the emergence of subharmonics ($f/2$ (b2), $f/4$ (b3), $f/8$ (b4)) at the x_f values shown on the figures, finally leading to chaotic oscillations at $x_f = 0.288$ (b5).

Figure 7 shows clearly that the system has several unstable attractors, making the trajectories of the system extremely complex. This is a common feature of nonlinear dynamical systems and has recently been observed in hydrodynamic systems as well [32]. As mentioned by Gibson *et al.* [32], once a system's unstable attractors have been determined, the next step is to determine how the system dynamics interconnects the neighbourhoods of these unstable attractors. We leave this for future work.

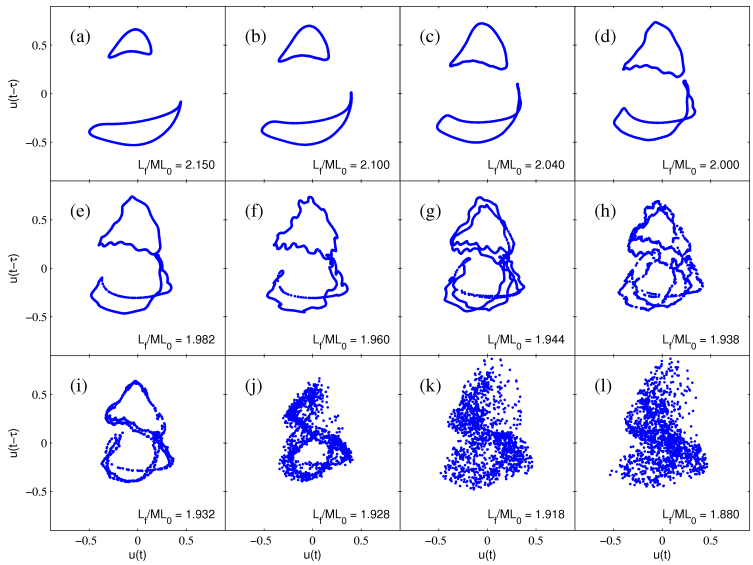

Figure 10: The Ruelle-Takens-Newhouse route to chaos observed in the L_f/ML_0 range of 1.88 to 2.15 (x_f = 0.4). (a) through (l) show the Poincaré sections of the final state. The quasi-periodic state (2-torus) in (a) develops corrugations on its surface due to stretching and folding (see (c), (d), (e) and (f)). This is followed by torus breakdown (see (g), (h) and (i)) to chaos (see (j), (k), (l)).

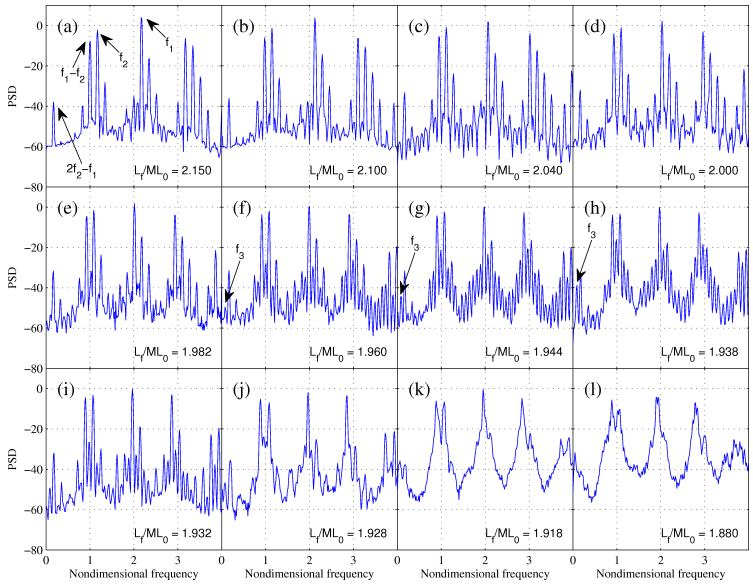

Figure 11: The Ruelle-Takens-Newhouse route to chaos (continued): (a) through (l) show the power spectra of u_f corresponding to the same subfigures in figure 10. This route to chaos is characterised by the emergence of a third frequency (see (f), (g) and (h)) that is incommensurate with the two frequencies of the quasi-periodic state (marked f_1 and f_2 in (a)).

2.4 Routes to chaos

If a nonlinear system exhibits chaotic dynamics it is natural to ask how this chaotic behaviour emerges as a parameter is varied. The three most common routes to chaos are via the period doubling cascade, the Ruelle-Takens-Newhouse route and intermittency [33]. In our study we have identified two routes to chaos: the period-doubling and the Ruelle-Takens-Newhouse routes.

Figures 8 and 9 show the period doubling cascade as the flame position is changed. On the left is the bifurcation diagram constructed using the negative peaks of the time series of u_f and on the right are the power spectra at flame locations just after each period doubling bifurcation. The first period doubling bifurcation from period-1 to period-2 oscillations is subcritical (not shown here) at $x_f = 0.307$. The arrows at $x_f = 0.308$ show that the transition to period-*2* oscillations is abrupt. The subsequent bifurcations occur at $x_f = 0.301$ (period 2 to 4) and $x_f = 0.296$ (period 4 to 8) and are supercritical. The power spectra on the right show the introduction of a subharmonic frequency at half the lowest frequency at each period-doubling bifurcation, ultimately leading to chaotic oscillations with a broadband spectrum and a few peaks at $x_f = 0.2861$.

Ruelle, Takens and Newhouse showed that three successive Hopf bifurcations, producing three independent frequencies, generates a 3-torus that can become unstable and be replaced by a strange attractor [33]. This route to chaos has been observed in recent experiments of a similar thermoacoustic system [2].

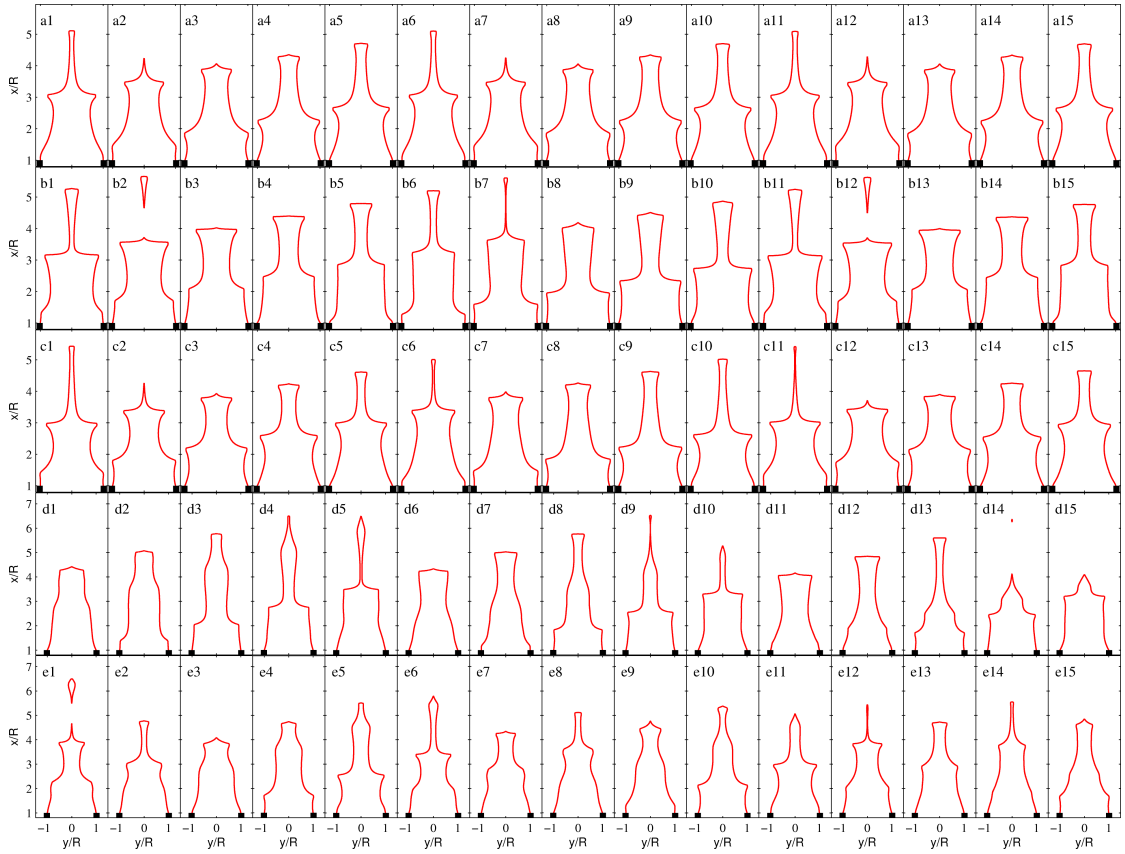

Figure 12: Instantaneous flame images of the self-excited flame for different types of oscillation: (a) period-*1* oscillation at $x_f = 0.435$ (mode-2 branch) (b) period-*2* oscillation at $x_f = 0.3$, (c) quasi-periodic oscillation at $x_f = 0.4$, (d) frequency-locked oscillation at $x_f = 0.286$ and (e) chaotic oscillation at $x_f = 0.4$. For (a) through (d) all other parameters are the same as in figure 3, while (e) has the same parameters as figure 6(e). 15 images are shown for each case spanning 3 cycles of the dominant frequency.

Figure 10 shows the Ruelle-Takens-Newhouse route to chaos as the natural acoustic frequency of the duct, L_f/ML_0, is changed. The Poincaré sections of phase portraits show that the initially stable quasi-periodic state (2-torus) in figure 10(a) develops corrugations on its surface (see figures 10(c), (d), (e) and (f)). The wrinkling of the surface of the attractor is characteristic of the two-fold operation leading to a strange attractor: stretching and folding. This is followed by torus breakdown (see figures 10(g), (h) and

(i)) to chaos (see figures 10 (j), (k), (l)). The power spectra of acoustic velocity at the flame position in figure 11 show the emergence of a third frequency (see figures 11(f), (g) and (h)) that is incommensurate with the two frequencies of the quasi-periodic state (marked f_1 and f_2 in figure 11(a)). This is a unique characteristic of the Ruelle-Takens-Newhouse route to chaos.

Figure 12 shows snapshots of the flame during different types of oscillation: (a) period-*1*, (b) period-*2* (c) quasiperiodic (d) frequency-locked and (e) chaotic. 15 images are shown for each case spanning 3 cycles of the dominant frequency. In (a) the snapshots 1-5, 6-10 and 11-15 are all identical, showing that the oscillation is indeed period-*1*. In (b) the snapshots 1-5 and 6-10 differ slightly but 11-15 are the same as 1-5, showing that the oscillation is period-*2*. Hence two cycles alternate here. In (c) a gradual shift in flame shapes can be seen across 1-5, 6-10 and 11-15, which shows a low frequency modulation of the dominant mode of oscillation. In (d) the behaviour is similar to (e), but the second frequency is exactly one-fifth of the first, hence the oscillation is periodic and the cycle repeats itself after 25 snapshots (not shown here). In (e) the oscillations are chaotic and the cycles never repeat themselves, however, the flame shapes have the same features as in the previous cases, *viz.* cusp formation and pinch-off.

These snapshots reflect the periodicity (or lack of it) in each type of oscillation. Further, they show that while the basic flame dynamics, such as cusp formation, advection of wrinkles along the flame and pinch-off at the tip, remain the same in all cases, clear differences exist in the shape of the cusps and the instants when they are formed at the base of the flame. This is because the generation of wrinkles at the base of the flame depends strongly on the acoustic velocity at the flame base, which in turn depends strongly on the type of oscillation. Finally, these flame shapes are similar to those in experiments, but lack the rounding off of cusps due to curvature and strain effects [3]. However, these experiments have also shown intermittency due to repeated flame lift-off and reattachment [3]. Such behaviour cannot be captured in this model because the flame remains attached to the burner at all times.

3 Conclusions

In this study a reduced order model of a ducted premixed flame is simulated and analysed using techniques from nonlinear time series analysis and dynamical systems theory.

The bifurcations of this system for varying flame position in the duct are identified. As the flame is moved from the centre of the duct to the entrance the system undergoes transition to period-*1* limit cycle oscillations via a subcritical Hopf bifurcation followed by subsequent bifurcations that lead to quasi-periodic, period-two, frequency-locked as well as chaotic oscillations. For certain parameter ranges more than one stable solution exists and the ultimate state reached depends on the initial conditions. Hence there is hysteresis and mode-switching is possible. The influence of the number of coupled acoustic modes on this behaviour is analysed. It is shown that a single mode assumption, which is equivalent to the describing function approach, underpredicts the oscillation amplitude in large regions of parameter space and fails to capture the bifurcations and multi-stability seen in the multi-modal case.

The phase portraits of the states of the system are reconstructed from the time series. The Poincaré sections of these phase portraits are shown to be powerful tools to identify the stable and unstable attractors. They show that the system often traverses through several intermediate states before reaching its final stable state. Further, two routes to chaos are established for this system: the period-doubling route and the Ruelle-Takens-Newhouse route and these are corroborated by analyses of the power spectra. Instantaneous snapshots of the oscillating flame show the multiple time and length scales of the flame wrinkles, which reveal the strongly non-harmonic behaviour of the time series.

This reduced order model with approximately 5000 degrees of freedom reproduces much of the rich behaviour seen in recent experiments on a similar thermoacoustic system and provides a tool to further investigate this nonlinear behaviour. The close correspondence between this model and low-dimensional chaotic dynamical systems will prove useful because the variety of results from dynamical systems can be brought to bear on thermoacoustics.

References

[1] L. Kabiraj and R. I. Sujith. Bifurcations of self-excited ducted laminar premixed flames. *J. Eng. Gas Turbines Power*, 134(031502), 2012.

[2] Lipika Kabiraj, Aditya Saurabh, Pankaj Wahi, and RI Sujith. Route to chaos for combustion instability in ducted laminar premixed flames. *Chaos*, 22(2):023129–023129, 2012.

[3] L. Kabiraj and R. I. Sujith. Nonlinear self-excited thermoacoustic oscillations: intermittency and flame blowout. *J. Fluid Mech.*, 713:376–397, December 2012.

[4] H. Gotoda, H. Nikimoto, T. Miyano, and S. Tachibana. Dynamic properties of combustion instability in a lean premixed gas-turbine combustor. *Chaos: An Interdisciplinary Journal of Nonlinear Science*, 21(1):013124–013124, 2011.

[5] James D Sterling. Nonlinear analysis and modelling of combustion instabilities in a laboratory combustor. *Combustion Science and Technology*, 89(1-4):167–179, 1993.

[6] Stephen B Margolis. Nonlinear stability of combustion-driven acoustic oscillations in resonance tubes. *Journal of Fluid Mechanics*, 253:67–67, 1993.

[7] Craig C Jahnke and Fred EC Culick. Application of dynamical systems theory to nonlinear combustion instabilities. *Journal of Propulsion and Power*, 10(4):508–517, 1994.

[8] S Lei and A Turan. Nonlinear/chaotic behaviour in thermo-acoustic instability. *Combustion Theory and Modelling*, 13(3):541–557, 2009.

[9] Santosh Hemchandra and Tim Lieuwen. Local consumption speed of turbulent premixed flames–an analysis of "memory effects". *Combustion and Flame*, 157(5):955–965, 2010.

[10] Iain C. Waugh. *Methods for analysis of nonlinear thermoacoustic systems*. PhD thesis, University of Cambridge, 2013.

[11] I. C. Waugh, K. Kashinath, and M. P. Juniper. Matrix-free continuation of limit cycles and their bifurcations for a ducted premixed flame. In *Summer school and workshop on Non-normal and Nonlinear effects in Aero- and Thermoacoustics*, 2013.

[12] A. P. Dowling. Nonlinear self-excited oscillations of a ducted flame. *J. Fluid Mech.*, 346(1):271–290, 1997.

[13] M. P. Juniper. Triggering in the horizontal Rijke tube: non-normality, transient growth and bypass transition. *J. Fluid Mech.*, 667:272–308, 2011.

[14] Priya Subramanian and R. I. Sujith. Non-normality and internal flame dynamics in premixed flame-acoustic interaction. *J. Fluid Mech.*, 679:315–342, 2011.

[15] K. Kashinath, S. Hemchandra, and M. P. Juniper. Nonlinear phenomena in thermoacoustic systems with premixed flames. *J. Eng. Gas Turbines Power (accepted)*, 2013.

[16] K. Kashinath, S. Hemchandra, and M. P. Juniper. Nonlinear thermoacoustics of ducted premixed flames: the influence of perturbation convection speed. *Combust. Flame (under review)*, 2013.

[17] L. Boyer and J. Quinard. On the dynamics of anchored flames. *Combust. Flame*, 82(1):51 – 65, 1990.

[18] F. Baillot, D. Durox, and R. Prud'homme. Experimental and theoretical study of a premixed flame. *Combust. Flame*, 88(2):149 – 168, 1992.

[19] Preetham, S. Hemchandra, and T. C. Lieuwen. Dynamics of laminar premixed flames forced by harmonic velocity disturbances. *J. Propul. Power*, 394(6):51–72, 2008.

[20] A. Birbaud, D. Durox, and S. Candel. Upstream flow dynamics of a laminar premixed conical flame submitted to acoustic modulations. *Combust. Flame*, 146(3):541 – 552, 2006.

[21] K.Kashinath, M. P. Juniper, and S. Hemchandra. Nonlinear phenomena in thermoacoustics: A comparison between single-mode and multi-mode methods. *Proceedings of the 19th International Congress on Sound and Vibration*, 2012.

[22] A. P. Dowling. A kinematic model of a ducted flame. *J. Fluid Mech.*, 394(1):51–72, 1999.

[23] S. Hemchandra. Premixed flame response to equivalence ratio perturbations: Comparison between reduced order modelling and detailed computations. *Combust. Flame*, 159:3530–3543, 2012.

[24] G. S. Jiang and D. Peng. Weighted eno schemes for hamilton-jacobi equations. *SIAM J. Sci. Comp.*, 21(6):2126–2143, 2000.

[25] S. Gottlieb and C. Shu. Total variation diminishing runge-kutta schemes. *Math. Comput.*, 67(221):73–86, 1998.

[26] D. Peng. A pde-based fast local level set method. *J. Comput. Phys.*, 155(2):410–438, 1999.

[27] S. Hemchandra. *Dyamics of turbulent premixed flames in acoustic fields*. PhD thesis, Georgia Institute of Technology, 2009.

[28] H. Kantz and T. Schreiber. *Nonlinear time series analysis*. Cambridge University Press, 2000.

[29] J. M. T. Thompson and H. B. Stewart. *Nonlinear dynamics and chaos*. John Wiley and Sons, Ltd., 2002.

[30] Peter Grassberger and Itamar Procaccia. Characterization of strange attractors. *Physical review letters*, 50(5):346–349, 1983.

[31] R. Hegger, H. Kantz, and T. Schreiber. Practical implementation of nonlinear time series methods: The tisean package. *Chaos*, 9(2):413–435, 1999.

[32] John Guckenheimer and Philip Holmes. *Nonlinear oscillations, dynamical systems, and bifurcations of vector fields*, volume 42. Springer-Verlag New York, 1983.

[33] J.F.Gibson, J.Halcrow, and P.Cvitanović. Equilibrium and travelling-wave solutions of plane couette flow. *J. Fluid Mech.*, 638(1):243–266, 2009.

[34] JP Eckmann. Roads to turbulence in dissipative dynamical systems. *Reviews of Modern Physics*, 53(4):643–654, 1981.